ФІЗИЧНІ, ХІМІЧНІ ТА ІНШІ ЯВИЩА, НА ОСНОВІ ЯКИХ МОЖУТЬ БУТИ СТВОРЕНІ СЕНСОРИ

PHYSICAL, CHEMICAL AND OTHER PHENOMENA, AS THE BASES OF SENSORS

PACS: 73.21.La, 73.22.-f, 71.35.-y
https://doi.org/10.18524/1815-7459.2026.2.360778

GEOMETRIC EFFECTS ON THE ENERGY SPECTRA OF CHARGE CARRIERS AND EXCITONS IN TETRAPOD-LIKE NANOSTRUCTURES

I. V. Bilynskyi[ab], https://orcid.org/0000-0002-4221-9225
R. Ya. Leshko[a], https://orcid.org/0000-0002-9072-164X
O. V. Leshko[a], https://orcid.org/0000-0001-9646-3189
Ya. Yu. Melnyk[b], https://orcid.org/0009-0007-7128-2024
A. V. Tymkiv[a], *P. P. Khomyn*[a]

[a] Department of Physics and Information Systems,
Drohobych Ivan Franko State Pedagogical University, 3 Stryiska St, Drohobych, 82100, Ukraine
[b] Department of Physics, Kryvyi Rih State Pedagogical University,
54 Universytetska St, Kryvyi Rih, 50086, Ukraine
e-mail: iv.bilynskyi@gmail.com; leshkoroman@gmail.com; leshkoolya9@gmail.com;
melnikyaroslav.qa@gmail.com; andrii.tymkiv@dspu.edu.ua; pavlo.homyn@dspu.edu.ua

Abstract. This paper presents a theoretical study of the energy spectra of electrons, holes, and excitons in tetrapod-shaped semiconductor quantum dots. To provide an adequate physical description of the complex three-dimensional morphology of the nanocrystals, three realistic macroscopic geometric models are proposed and systematically compared. The calculations are performed within the effective mass approximation using a finite potential barrier model. The numerical solution of the stationary Schrödinger equation for single-particle electron and hole states, as well as the calculation of the total exciton energy, is carried out using the Finite Element Method. It is established that the spatial overlap at the geometric core-arm junction determines the regime of strong spatial quantum confinement. The analysis of the results reveals a complex non-monotonic dependence of the electron and exciton ground-state energies on the height of the tetrapod arms. This behavior is driven by a strong physical competition between the localization of charge carriers within the central core and their penetration into the available volume of the epitaxial arms. It is demonstrated that when the core volume dominates, the geometric narrowing at the junction creates an effective potential barrier that locks the carrier wave function in the center of the nanostructure, inevitably leading to an increase in energy. Conversely, it is convincingly shown that the fundamental exciton transition energy is practically independent of the overall arm length and is primarily determined by the core radius and the arm thickness. The theoretical results from the cylindrical model demonstrate excellent quantitative agreement with the optical spectroscopy data of synthesized long-arm CdSe tetrapod. The discrepancy observed for short-arm tetrapod highlights the sensitivity of the energy spectrum to surface states and structural imperfections at the nanoscale.

Keywords: tetrapod-like quantum dot; exciton; electron and hole energy spectrum

1. INTRODUCTION

Tetrapod-shaped semiconductor quantum dots (QDs) attract significant attention in the fields of computational nanophysics and materials science due to their unique characteristics, which open up broad possibilities for applications in modern nanotechnologies. Their branched three-dimensional structure, consisting of a central core and four epitaxially grown arms, creates conditions for strong and asymmetric quantum confinement of electrons, holes, and excitons. Due to the ability to fine-tune the energy spectrum, such nanostructures (particularly GaAs/AlGaAs) are highly promising for the development of high-speed optoelectronic devices, infrared detectors, and quantum computing systems, where nonlinear optical effects, such as nonlinear optical rectification, play a significant role [1, 2]. Furthermore, the ability of the tetrapod arms (for example, in CdSe/CdS structures) to act as dynamic levers allows them to transform local mechanical strains into shifts in photoluminescence peaks, making them ideal nanoscale strain gauges [3, 4]. The integration of such fluorescent probes into polymer matrices enables the creation of "smart" nanocomposites for the precise measurement of microscopic mechanical stresses with a high dynamic range, which is of importance for both fundamental biomechanics and monitoring the structural integrity of materials [5].

The formation of complex tetrapod-shaped nanostructures is the result of fine control over crystallographic polymorphism during colloidal synthesis [6]. The process is typically initiated by the nucleation of a central core in the cubic zinc blende phase. Since the {111} facets of this cubic lattice are structurally equivalent to the basal planes of the hexagonal wurtzite phase, they serve as ideal nucleation sites for the epitaxial growth of the arms. By rapidly changing thermodynamic conditions (specifically, temperature and precursor concentration), the reaction is driven into a strict kinetic regime. This stimulates the rapid anisotropic growth of four hexagonal arms along the c-axes, while thermodynamically blocking further isotropic growth of the cubic core itself. Such a mechanism allows for precise and independent control over both the diameter of the central core and the geometric parameters (length and thickness) of the arms, which is a critical tool for the spatial engineering of wave functions and tuning the energy spectrum of charge carriers in such heterostructures. Furthermore, the introduction of transition metal impurities, such as copper, into the base CdSe structures allows for additional modification of their nonlinear optical characteristics and control over photoluminescence processes [7, 8].

From a theoretical perspective, accurately modeling the electronic structure and excitonic states of tetrapod-shaped QDs requires sophisticated numerical approaches due to their complex three-dimensional geometry. Initial computational studies focused on determining the energy spectra of electrons, holes, and excitons in bare II-VI tetrapods, such as CdTe, utilizing the effective mass approximation and 3D numerical solutions. These studies demonstrated how the spatial localization of charge carriers sensitively transitions between the central core and the arms depending on the geometric dimensions of the structure [9, 10]. Furthermore, theoretical frameworks were subsequently extended to complex core-shell architectures (e.g., CdTe/CdS tetrapods) by incorporating continuum elasticity theory. This allowed researchers to calculate the spatial distribution of internal mechanical stresses caused by lattice mismatch, which modifies the band alignment and the overall optical properties of the nanocrystals [11]. More recently, the theoretical analysis of these nanostructures has been generalized to account for external macroscopic perturbations. For instance, detailed computational models have been employed to evaluate the photoionization cross-section, revealing how variations in hydrostatic pressure, temperature, and the polarization direction of the incident light critically impact the optical transitions and electronic confinement within tetrapod QDs [12].

Building upon these theoretical foundations, the exact geometric representation of the tetrapod structure remains an important factor in accurately

determining the energy states. In a recent study [13], a geometric model of a tetrapod-like QD was proposed where the arms were approximated as spheres with their centers located precisely on the surface of a central spherical core. However, a primary limitation of this approach was the strict dimensional constraint applied to the arm radii to prevent their spatial intersection. To overcome this limitation and provide a more physically realistic description of the nanostructures, the aim of the present work is to investigate the energy spectra of electrons, holes, and excitons in tetrapod QDs by employing and comparing more advanced structural models. Specifically, we explicitly account for the mutual intersection of the arms in the modified spherical-arm configuration and introduce an alternative conical-arm and cylindric-arm model. In those novel geometries, the central core remains a sphere (or absent), while the four arms are modeled as cones (or cylinders) whose theoretical vertices converge at the exact center of the core. The calculations of the single-particle and excitonic states for both geometric configurations are performed numerically using the Finite Element Method (FEM). Therefore the main aim of this manuscript is systematically comparing the resulting energy states between these distinct morphological models, this study aims to demonstrate how the geometric shape of the arms and their interfacial overlap affect the spatial confinement of charge carriers and the overall optical properties of the system.

2. TETRAPOD MODEL

To calculate the energy states of charge carriers (electrons and holes) in tetrapod-shaped QDs, we employ the single-band effective mass approximation. The spatial confinement of the carriers is described by a three-dimensional rectangular potential barrier model. Within this framework, the single-particle Hamiltonian for an electron or a hole is written

$$\hat{H}=-\frac{\hbar^2}{2}\vec{\nabla}\cdot\left(\frac{1}{m(\vec{r})}\vec{\nabla}\right)+U(\vec{r}), \qquad (1)$$

where ħ is the reduced Planck constant, and m is the position-dependent effective mass of the charge carrier, which takes distinct values inside the semiconductor nanostructure and in the surrounding matrix. The confinement potential U is modeled as a finite 3D rectangular well, defined as $U = 0$ inside the tetrapod domain and $U = U_0$ outside the structure, where U_0 is the barrier height determined by the band alignment of the chosen materials.

The complex three-dimensional morphology of the tetrapod QD is defined by a central core and four symmetric arms oriented along the axes of a regular tetrahedron. To systematically investigate the influence of the nanostructure's shape on the carrier energy spectra, we consider two distinct geometric models.

A. The Intersecting Spheres Model

In the first configuration, the tetrapod is constructed as a union of five spherical domains. The central core is represented by a sphere of radius a_{core} centered at the origin of the coordinate system at (0,0,0). The four arms are modeled as identical spheres of radius a_{arm}. The centers of these four arm-spheres are distributed symmetrically along the four tetrahedral directions. Unlike previous restricted models [13], this configuration explicitly allows and accounts for the spatial intersection of the arm-spheres both with the central core and with one another (Fig. 1a). This mutual overlap creates a continuous, complex morphological boundary that naturally reflects the volumetric blending of the arms during growth.

B. The Conical-Arm Model

The second configuration provides an alternative morphological representation, combining a central spherical core with conical arms. Here, the central core remains a sphere of radius a_{core} located at the origin. The four arms are modeled as identical circular cones, each characterized by a height H and a base radius a_{base}. A defining feature of this model is that the theoretical vertices of all four cones converge exactly at the center of the core (the origin). Consequently, the height H is measured from the origin to the center of the cone's base along its central axis. The central axes of these cones are aligned with the four tetrahedral directions. The physically meaningful domain of the tetrapod is

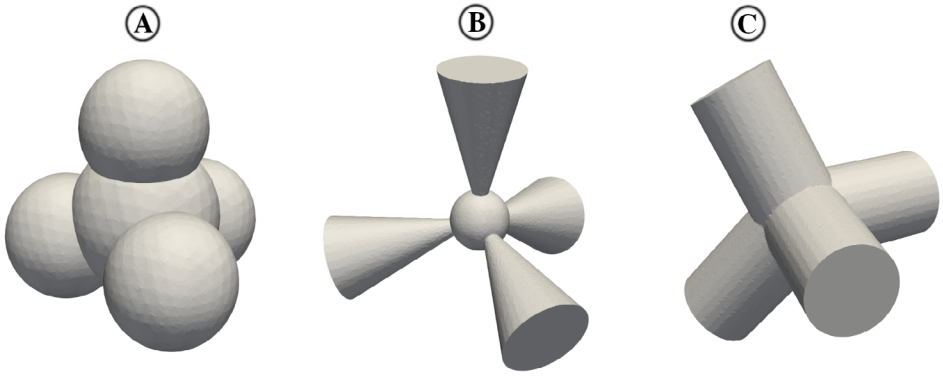

Figure 1. Geometric models of tetrapods.

thus formed by the union of the central sphere and the expanding volumes of the cones that protrude beyond the core's surface (Fig. 2b). This geometric model closely mimics the epitaxial growth dynamics, where the arm cross-section gradually increases from the nucleation center outward.

C. The Cylindrical-Arm Model.

The third configuration presents a geometric model consisting exclusively of four intersecting cylindrical arms, without a distinct central spherical core. The arms are modeled as four identical right circular cylinders, each defined by a length L (measured from the center of the structure) and a constant cross-sectional radius a_{cyl}. The longitudinal axes of these cylinders are aligned strictly with the four symmetric tetrahedral directions, converging directly at the origin (0,0,0). The physically meaningful domain of the tetrapod is formed by the spatial union of these four cylindrical volumes, which naturally creates a branched central junction through their mutual intersection. This model accurately represents the morphology of highly anisotropic, elongated tetrapods typically obtained in colloidal synthesis, where the wurtzite arms maintain a nearly constant diameter along their entire epitaxial growth axis and seamlessly fuse at the nucleation center.

To determine the electron and hole energy spectra, the stationary Schrödinger equation with the Hamiltonian (1) must be solved. Due to the complex, non-trivial boundaries of the intersecting spheres and conical-arm models, analytical solutions are not feasible. Therefore, the calculations of the single-particle and excitonic states for both geometric configurations are performed numerically using the FEM. In our work, this numerical approach is implemented using the FEniCS open-source computing platform. The 3D physical domain of the quantum dot and the surrounding matrix is discretized into an unstructured tetrahedral mesh. The continuous stationary Schrödinger equation is then transformed into its weak variational form. This reduces the differential equation to a sparse generalized algebraic eigenvalue problem, which is solved to obtain the energy levels (eigenvalues) and the corresponding 3D probability density distributions (wave functions) for the electrons and holes.

For the correlated electron-hole pair (exciton), the physical model must account for the electrostatic attraction between the charge carriers. The corresponding exciton Hamiltonian is constructed by combining the single-particle Hamiltonians (1) with the Coulomb interaction term:

$$\hat{H}_{exc}=\hat{H}_e(\vec{r}_e)+\hat{H}_h(\vec{r}_h)-\frac{e^2}{4\pi\varepsilon_0\varepsilon|\vec{r}_e-\vec{r}_h|}, \qquad (2)$$

where $\hat{H}_e(\vec{r}_e)$ and $\hat{H}_e(\vec{r}_h)$ are the single-particle operators for the electron and hole in form (1), respectively, e is the elementary charge, ε_0 is the vacuum permittivity, and ε is the average dielectric permittivity of the heterostructure.

Because a direct numerical solution of the full 6D two-particle Schrödinger equation is computationally prohibitive for such complex geom-

etries, we employ a self-consistent iterative procedure based on the coupled Schrödinger-Poisson system. The calculation of the excitonic state is performed within the mean-field approximation using the FEM through the following algorithm. Initially, the single-particle stationary Schrödinger equation is solved for the electron (assuming no hole is present) to determine its unperturbed ground-state wave function, $\Psi_e(\vec{r})$. Using this wave function, the spatial charge density of the electron is evaluated. Subsequently, the 3D Poisson equation is solved numerically to find the electrostatic potential $\Phi_e(\vec{r})$ generated by the electron distribution:

$$\vec{\nabla} \cdot \left(\varepsilon_0 \varepsilon \vec{\nabla} \Phi_e(\vec{r})\right) = e|\Psi_e(\vec{r})|^2. \quad (3)$$

The resulting Coulomb potential energy, $V_{eh}(\vec{r}) = -e\Phi_e(\vec{r})$, is then incorporated into the single-particle Hamiltonian of the hole as an additional attractive confinement term. The modified Schrödinger equation for the hole is solved to obtain its localized wave function, $\Psi_h(\vec{r})$.

In the next step, the charge density of the hole is computed to solve the corresponding Poisson equation for the hole-generated electrostatic potential. This new potential is then fed back into the electron's Schrödinger equation, updating its potential energy landscape.

This coupled Schrödinger-Poisson iterative loop is continuously repeated, recalculating the wave functions and potentials at each step, until the energy eigenvalues of both the electron and the hole converge within a strictly predefined numerical tolerance. Once self-consistency is achieved, the total ground-state energy of the exciton is calculated by summing the converged kinetic and potential energies of the interacting charge carriers.

In the final step, once self-consistency is achieved, the total ground-state energy of the exciton E_{ex} is calculated. It is important to note that the converged single-particle eigenvalues for the electron E_e and the hole E_h both inherently include the Coulomb interaction energy. Therefore, a direct summation of these eigenvalues would result in double-counting the electron-hole electrostatic attraction. To obtain the correct total energy of the excitonic state, this interaction energy must be subtracted:

$$E_{exc} = E_e + E_h - E_C, \quad (4)$$

where E_C is the Coulomb interaction energy of the electron-hole pair. In the framework of our computational model, this term is calculated by integrating the hole probability density over the effective Coulomb potential landscape generated by the electron:

$$E_C = \int_V V_{eh}(\vec{r})|\Psi_h(\vec{r})|^2 d\vec{r}. \quad (5)$$

Therefore, the exciton energy has been calculated.

III. ANALYSIS OF THE OBTAINED RESULTS

The proposed geometric models of tetrapods, evaluated numerically using the FEM in FEniCS, were applied to calculate the energy states of a CdSe tetrapod quantum dot embedded in an organic matrix. For the QD, the effective masses are $m_e = 0.11 m_0$ and $m_h = 0.44 m_0$ [10,13], the dielectric permittivity is ε=9.6, and the band gap is E_g=1.74 eV [10]. In the surrounding organic matrix, the carrier masses are assumed to be $m_e = m_h = m_0$. The environmental influence at the phase interface is accounted for through a finite-height potential barrier. Due to the marked disparity in ionization energies and electron affinities between the semiconductor and the organic medium, the barrier heights were set to U_e=4 eV for electrons and U_h=2 eV for holes.

Initially, we considered the first geometric configuration, where the tetrapod is modeled as a system of intersecting spheres. A similar geometric model was previously proposed in [13], where the electron, hole, and exciton energy spectra were calculated using the plane wave expansion method. However, a primary limitation of that earlier approach was the dimensional constraint applied to the arm radii to prevent their spatial intersection. Specifically, to avoid the overlapping of the peripheral spherical arms, the geometric parameters were mathematically restricted to the condition $a_{\text{arm}} \leq 0.816\, a_{core}$. In this

work we do not use this condition. To validate our current computational framework, we calculated the single-particle states within this restricted, non-intersecting regime. The results of our numerical modeling, obtained using the FEM in FEniCS in this work, perfectly coincide with the data derived from the plane wave method in [13]. The corresponding comparative analysis of the energy spectra is illustrated in the Fig. 2 below.

In the presented Fig 2, the vertical solid line indicates the critical arm radius that separates two distinct geometric regimes. To the left of this line, the arm spheres do not intersect with one another, corresponding to the strict geometric constraint established in our previous work [13]. Within this region, the energy spectra calculated using both the FEM and the plane wave expansion method from [13] are shown to be in perfect agreement. To the right of the vertical line, the arms begin to spatially intersect. Because the plane wave approach in [13] was limited to the non-intersecting configuration, the energy states in this overlapping regime are computed exclusively using the FEM developed in the present study.

A completely analogous comparative analysis was performed for the hole energy states. The results similarly demonstrated excellent agreement between the two numerical techniques in the non-intersecting regime, although the corresponding graphical representation is omitted here for brevity.

Having successfully validated our FEM approach and confirmed its consistency with the plane wave method for the five-sphere model (Geometry A), we can confidently extend our numerical framework to investigate the alternative morphological configuration. Consequently, the validated FEM is subsequently applied to calculate the both electron and exciton states in the conical-arm tetrapod model (Geometry B) and cylindrical-arm model (Geometry C).

Fig. 3 presents the non-monotonic dependence of the electron ground-state energy on the height of the conical arms H. The overall difference between the curves is governed by the quantum confinement effect: a smaller core radius a_{core} confines the electron wave function more strongly, which naturally shifts the entire energy spectrum upwards. The non-monotonicity itself is determined by the competition between the core and the arms. If the cone base radius is comparable to the core, a transitional geometry forms at small H, hindering the electron's penetration into the arms, so the energy initially increases, as the electron density spreads into the arms (see inset 3, Fig. 3). Only when the cones elongate

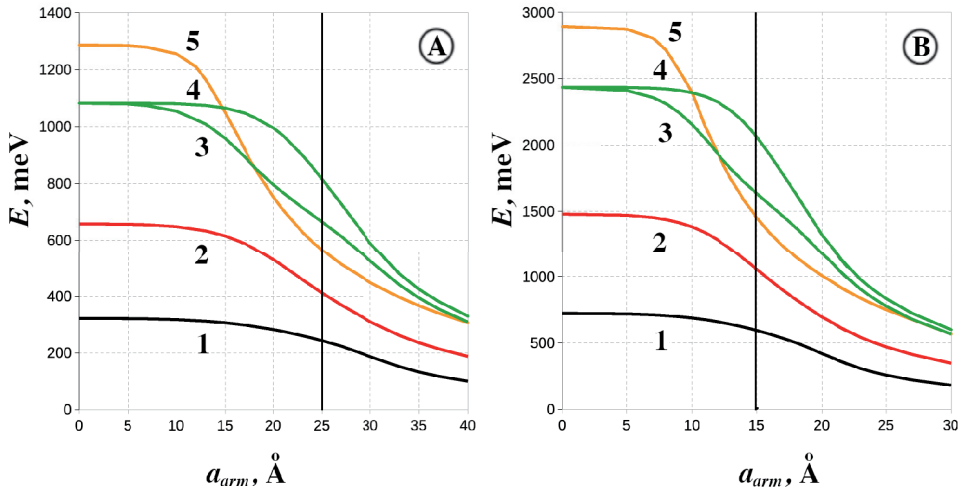

Figure 2. Electron energy spectra in the tetrapod QD as a function of tetrapod arm radius with fixed core radius. A – core radius a_{core} = 30 Å, B – core radius a_{core} = 20 Å. Black curve (1) corresponds to the ground 1s-state; red curve (2) corresponds to the first 1p-state; green curves (3,4) represent the split components of the first 1d-states; orange curve (5) is the first excited 2s-state.

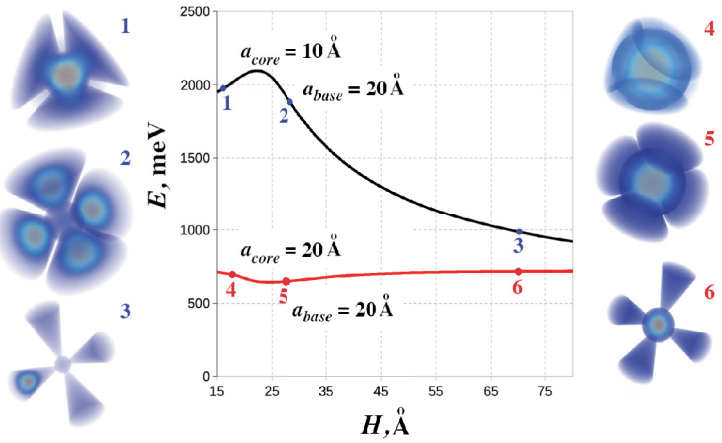

Figure 3. Electron ground-state energy in the conical-arm tetrapod QD as a function of the arm height H for different core sizes. The arm base radius is fixed at a_{base} = 20 Å. The left and right insets visualize the 3D spatial distribution of the electron probability density for the specific geometric configurations marked by numbers 1, 2, 3, 4, 5, and 6 on the energy curves.

sufficiently, increasing the available volume, does the energy begin to decrease. In contrast, if a larger core dominates over a narrow cone base, the electron density is always concentrated in the center. As long as the cone grows within the sphere, the confinement is slightly relaxed, and the energy locally drops. However, once the arms protrude outward, the aperture of their intersection with the core constantly narrows. This creates an effective geometric barrier that strictly locks the electron within the core (visualized in insets 1 and 2 Fig. 3), leading to a rapid increase in energy.

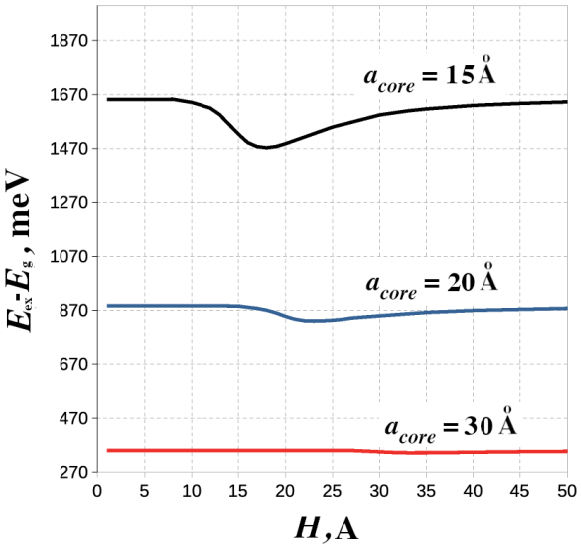

Figure 4. Exciton ground-state energy in the conical-arm tetrapod QD as a function of the arm height H for different core sizes. The arm base radius is fixed at a_{base} = 15 Å.

The revealed localization patterns of the individual charge carriers directly determine the behavior of the exciton energy. Since the total ground-state energy of the exciton comprises the single-particle energies of the electron and the hole minus their mutual Coulomb attraction, the non-monotonic behavior of the carriers (governed by the competition between the core and arm volumes) leads to a similar dependence of the exciton energy on the height H. Furthermore, the analysis demonstrates that at sufficiently large values of H, the exciton energy practically ceases to depend on the cone height (the length of the arms). Instead, it is predominantly determined by the core radius and the arm thickness (the base radius). This theoretical finding is in excellent agreement with experimental observations [7, 8], which confirmed that the fundamental exciton transition energy in tetrapod-shaped nanocrystals is dictated by the arm thickness rather than their overall length.

A more realistic morphological representation for synthesized colloidal nanocrystals is provided by a tetrapod model consisting of four cylindrical arms (Geometry C). We performed numerical simulations of the energy states using cylindrical parameters that correspond to the experimental data reported in Refs. [7, 8]. To facilitate a direct comparison with the optical spectroscopy measurements, the calculated ground-state exciton energies were converted into the

corresponding wavelengths λ_{ex}. These theoretical results, alongside the experimental values for the investigated samples, are summarized in Table 1.

Table 1

Ground-state exciton energy of tetrapod QD

Sample	λ_{ex}, nm (theory)	λ_{ex}, nm (experiment [7-8])
Long-arm tetrapod CdSe (L = 80 Å, a_{cyl} = 25Å)	535.56	535.00
Short-arm tetrapod CdSe (L = 45 Å, a_{cyl} = 25Å)	615.59	552.00

For the long-arm sample, the theoretical and experimental results agree within 0.1%, confirming the adequacy of the proposed cylindrical model. In contrast, for the short-arm tetrapod, the discrepancy is 11.5%. This difference is due to the extreme sensitivity of the exciton energy to the arm thickness, coupled with significant experimental measurement uncertainty (±0.5 nm tolerance for the width [7, 8]). Furthermore, in small nanocrystals, the wave function is highly sensitive to surface states and deviations from an ideal cylindrical shape at the core-arm junction, which makes the actual spatial confinement somewhat weaker than assumed in the strict theoretical model.

A comparison of three different nanostructures with the same total volume (a cylindrical-short-arm tetrapod, a spherical-arm tetrapod with a_{core} = 32 Å, a_{arm} = 23.5 Å, and a simple spherical QD R = 40.5 Å) clearly demonstrates the decisive influence of geometric shape on the quantum confinement effect. Despite the identical amount of semiconductor material, the branched spatial morphology of both tetrapod models creates significantly stronger conditions for charge carrier localization compared to an ideal sphere. Consequently, the simple spherical structure is characterized by the weakest spatial confinement and the longest exciton transition wavelength 649.92 nm, whereas the complex tetrapod-like geometries induce an increase in energy and a corresponding blue shift in the spectrum (specifically, to 623.15 nm for the spherical-arm model).

IV. CONCLUSIONS

In this work, we theoretically investigated the energy spectra of charge carriers and excitons in tetrapod-shaped QDs using the FEM. We proposed and compared three realistic geometric configurations: intersecting spheres, conical arms, and cylindrical arms, which accurately reflect the morphology of synthesized nanocrystals. The numerical calculations confirmed that the geometric shape and the degree of spatial overlap at the core-arm interface determine the quantum confinement regime.

Our analysis revealed a non-monotonic dependence of the electron and exciton ground-state energies on the height of the tetrapod arms. This complex behavior is driven by the physical competition between the carrier localization in the central core and their penetration into the expanding arm volumes. Specifically, the narrowing of the intersection aperture during growth can create an effective geometric barrier that strongly locks the charge carriers within the core.

Furthermore, we demonstrated that the fundamental exciton transition energy is predominantly determined by the core radius and arm thickness, rather than the overall arm length. The results obtained for the cylindrical-arm model showed excellent quantitative agreement with experimental optical spectroscopy data for long-arm CdSe tetrapod. For short-arm nanocrystals, the observed theoretical discrepancies highlight the extreme sensitivity of the energy spectrum to surface states and structural imperfections at the nanoscale.

REFERENCES

[1]. Cherni A., Zeiri N., Hayrapetyan D. B., Ed-Dahmouny A., El Sayed M. E., Samir A., Duque C. A. Machine learning models for predicting the hydrogenic impurity nonlinear optical rectification in GaAs/AlGaAs Tetrapod core/shell quantum dots under the effect of temperature. Materials Today Physics. 2025. Vol. 58. P. 101833. https://doi.org/10.1016/j.mtphys.2025.101833.

[2]. Zeiri N., Ed-Dahmouny A., Hayrapetyan D. B., Başer P., Sali A., El Sayed M. E., Samir A., Duque C. A. Machine learning-based prediction of nonlinear optical rectification in GaAs/AlGaAs tetrapod core/shell quantum dots under pressure and central hydrogenic impurity effects. Materials Science in Semiconductor Processing. 2025. Vol. 200. P. 110010. https://doi.org/10.1016/j.mssp.2025.110010.

[3]. Raja S. N., Olson A. C. K., Thorkelsson K., Luong A. J., Hsueh L., Chang G., Gludovatz B., Lin L., Xu T., Ritchie R. O., Alivisatos A. P. Tetrapod Nanocrystals as Fluorescent Stress Probes of Electrospun Nanocomposites. Nano Letters. 2013. Vol. 13, no. 8. P. 3915–3922. https://doi.org/10.1021/nl401999t.

[4]. Choi C. L., Koski K. J., Olson A. C., Alivisatos A. P. Luminescent nanocrystal stress gauge. Applied Physical Sciences. 2010. Vol. 107, no. 50. P. 21306–21310. https://doi.org/10.1073/pnas.1016022107.

[5]. Raja S. N., Ye X., Jones M. R. et al. Microscopic mechanisms of deformation transfer in high dynamic range branched nanoparticle deformation sensors. Nature Communication. 2018. Vol. 9. P. 1155:1–10. https://doi.org/10.1038/s41467-018-03396-5.

[6]. Manna L., Milliron D., Meisel A. et al. Controlled growth of tetrapod-branched inorganic nanocrystals. Nature Mater. 2003. Vol. 2. P. 382–385. https://doi.org/10.1038/nmat902.

[7]. Smirnov A. M., Golinskaya A. D., Kotin P. A., Dorofeev S. G., Palyulin V. V., Mantsevich V. N., Dneprovskii V. S. Photoluminescence and nonlinear transmission of Cu-doped CdSe quantum dots. Journal of Luminescence. 2019. Vol. 213. P. 29–35. https://doi.org/10.1016/j.jlumin.2019.05.001.

[8]. Smirnov A. M., Golinskaya A. D., Kotin P. A., Dorofeev S. G., Zharkova E. V., Palyulin V. V., Mantsevich V. N., Dneprovskii V. S. Damping of Cu-Associated Photoluminescence and Formation of Induced Absorption in Heavily Cu-Doped CdSe Quantum Dots. The Journal of Physical Chemistry C. 2019. Vol. 123, no. 45. P. 27986–27992. https://doi.org/10.1021/acs.jpcc.9b09918.

[9]. Sakoda K., Yao Y., Kuroda T., Dirin D. N., Vasiliev R. B. Exciton states of CdTe tetrapod-shaped nanocrystals. Optical Materials Express. 2011. Vol. 1, no. 3. P. 379–390. https://doi.org/10.1364/OME.1.000379.

[10]. Yao Y., Kuroda T., Dirin D. N., Irkhina A. A., Vasiliev R. B., Sakoda K. Exciton states of II-VI tetrapod-shaped nanocrystals. Optical Materials Express. 2013. Vol. 3, no. 7. P. 977–987. https://doi.org/10.1364/OME.3.000977.

[11]. Yao Y., Kuroda T., Dirin D. N., Sokolikova M. S., Vasiliev R. B. Strain effects on optical properties of tetrapod-shaped CdTe/CdS core-shell nanocrystals. Superlattices and Microstructures. 2014. Vol. 76. P. 244–252. http://dx.doi.org/10.1016/j.spmi.2014.10.017.

[12]. Ed-Dahmouny A., Althib H. M., Alkhaldi A., El Kharrim A., Jaouane M., Arraoui R., Fakkahi A., Zeiri N., Sali A., Duque C. A. Photoionization Cross-Section in Tetrapod Quantum Dots: Impact of Pressure, Temperature, and Polarization Direction. Adv. Theory Simul. 2025. Vol. 8, no. 12. P. e01286. https://doi.org/10.1002/adts.202501286.

[13]. Leshko R. Ya., Leshko O. V., Bilynskyi I. V., Melnyk Ya. Yu., Ocheretyanyi A. O., Chekin O. I., Kvyk M. V. Energy spectrum of electrons, holes, and excitons in tetrapod-like quantum dots. Physics Letters A. 2026. Vol. 587. P. 131726. https://doi.org/10.1016/j.physleta.2026.131726.

Стаття надійшла до редакції: 13.05.2026
прийнята до друку: 01.06.2026
опублікована: 30.06.2026

PACS: 73.21.La, 73.22.-f, 71.35.-y
https://doi.org/10.18524/1815-7459.2026.2.360778

ВПЛИВ ГЕОМЕТРІЇ НА ЕНЕРГЕТИЧНІ СПЕКТРИ НОСІЇВ ЗАРЯДУ ТА ЕКСИТОНІВ У ТЕТРАПОДОПОДІБНИХ НАНОСТРУКТУРАХ

І. В. Білинський[ab], Р. Я. Лешко[a], О. В. Лешко[a], Я. Ю.Мельник[b], А. В. Тимків[a], П. П. Хомин[a]
[a] Кафедра фізики та інформаційних систем,
Дрогобицький державний педагогічний університет імені Івана Франка,
вул. Стрийська 3, Дрогобич, 82100, Україна
[b] Кафедра фізики, Криворізький державний педагогічний університет,
вул. Університетська 54, Кривий Ріг, 50086, Україна
e-mail: iv.bilynskyi@gmail.com; leshkoroman@gmail.com; leshkoolya9@gmail.com;
melnikyaroslav.qa@gmail.com; andrii.tymkiv@dspu.edu.ua; pavlo.homyn@dspu.edu.ua

Анотація. У цій роботі представлено теоретичне дослідження енергетичних спектрів електронів, дірок та екситонів у тетраподоподібних напівпровідникових квантових острівцях. Для забезпечення адекватного фізичного опису складної тривимірної морфології нанокристалів запропоновано та систематично порівняно три реалістичні макроскопічні геометричні моделі. Розрахунки виконано в наближенні ефективної маси з використанням моделі скінченного 3D потенціального бар'єра. Чисельне розв'язання стаціонарного рівняння Шредінгера для одночастинкових електронних та діркових станів, а також розрахунок повної енергії екситона, здійснено за допомогою методу скінченних елементів. Встановлено, що просторове перекриття на геометричному стику ядро-рукав визначає режим сильного просторового квантового обмеження. Аналіз результатів виявляє складну немонотонну залежність енергій основного стану електрона та екситона від висоти рукавів тетрапода. Така поведінка зумовлена сильною фізичною конкуренцією між локалізацією носіїв заряду всередині центрального ядра та їхнім проникненням у доступний об'єм епітаксіальних рукавів. Продемонстровано, що коли домінує об'єм ядра, геометричне звуження на стику створює ефективний потенціальний бар'єр, який жорстко замикає хвильову функцію носіїв у центрі наноструктури, що неминуче призводить до зростання енергії. Натомість переконливо показано, що енергія основного екситонного переходу практично не залежить від загальної довжини рукавів і визначається переважно радіусом ядра та товщиною рукавів. Теоретичні результати, отримані з використанням циліндричної моделі, демонструють відмінний кількісний збіг з даними оптичної спектроскопії синтезованих довгорукавних квантових острівців CdSe. Розбіжність, що спостерігається для короткорукавних зразків, підкреслює чутливість енергетичного спектра до поверхневих станів та структурних недосконалостей на нанорівні.

Ключові слова: тетраподоподібний квантовий острівець; екситон; електронний і дірковий спектр